coatings

MDPI

Article

Study on Friction and Wear Characteristics of Axial Piston Pump Valve Plate Pairs Modified with Different Surface Energies

Yingna Liang [1,2,*], Wei Wang [1,2], Miaomiao Shen [1,2], Zhepeng Zhang [1,2], Hao Xing [1,2], Cunyuan Wang [1,2] and Dianrong Gao [1,2,*]

[1] School of Mechanical Engineering, Yanshan University, Qinhuangdao 066004, China; 17734387375@163.com (W.W.); sapling98@163.com (M.S.); z18833836096@163.com (Z.Z.); 15236648608@163.com (H.X.); wangcunyuan2022@163.com (C.W.)
[2] State Key Laboratory of Lifting Machinery, Yanshan University, Qinhuangdao 066004, China
* Correspondence: liangyingna@ysu.edu.cn (Y.L.); gaodr@ysu.edu.cn (D.G.)

Abstract: To explore the friction and wear performance of the valve pair with different wetting combinations under various working conditions in hydraulic oil lubrication, a low surface energy modification method was adopted in this paper to improve the surface wettability of the upper sample composed of SAF2507 and the lower sample composed of CFRPEEK, and to prepare valve plate pairs with different wetting combinations. The MMU-5G friction and wear testing machine was used to investigate its friction and wear characteristics under hydraulic oil lubrication. The results show that the surface free energy of SAF2507 and CFRPEEK decreased significantly after the treatment with a low surface energy solution, and the surface free energy of the upper and lower samples decreased by 41.9% and 42.2%, respectively. The oil contact angle of samples remained lipophilic, but the oil contact angle increased significantly. Under the working condition of low speed (800 r/min), the surface wettability of the valve plate pair has a great influence on its friction and wear characteristics. When operating at high speed (1200 r/min), the surface wettability of the valve plate pair has little influence on its friction and wear characteristics.

Keywords: friction and wear characteristics; valve plate pair; wettability

check for updates

Citation: Liang, Y.; Wang, W.; Shen, M.; Zhang, Z.; Xing, H.; Wang, C.; Gao, D. Study on Friction and Wear Characteristics of Axial Piston Pump Valve Plate Pairs Modified with Different Surface Energies. *Coatings* **2024**, *14*, 328. https://doi.org/10.3390/coatings14030328

Academic Editor: Ludmila B. Boinovich

Received: 13 February 2024
Revised: 7 March 2024
Accepted: 8 March 2024
Published: 10 March 2024

Copyright: © 2024 by the authors. Licensee MDPI, Basel, Switzerland. This article is an open access article distributed under the terms and conditions of the Creative Commons Attribution (CC BY) license (https://creativecommons.org/licenses/by/4.0/).

1. Introduction

The axial piston pump is a kind of positive volumetric hydraulic pump, which can convert mechanical power into hydraulic power. It is widely used in aerospace, machinery, shipbuilding and other fields because of its compact structure, high functional density, high reliability, easy automatic assembly and long service life [1–3].

The valve plate pair is one of the key friction pairs of axial piston pumps, and its reasonable design is very important. It is found that one of the most common failures of mechanical parts is wear and tear [4], the oil pump distribution friction pair will fail due to wear [5–7]. Therefore, reducing the friction loss of the valve plate pair can improve the service life of the pump. Selecting appropriate materials is an effective way to improve wear resistance. Among them, the valve plate pair composed of special polymer carbon fiber-reinforced polyetheretherketone (CFRPEEK) as the valve plate material and super duplex stainless steel $Cr_{25}Ni_7Mo_4N_{0.27}$ (SAF2507) as the cylinder liner material is a common form [8].

The preparation of a high-wear-resistant coating on the surface of the material is one of the effective strategies to reduce wear. Lui et al. [9] used an Fe-Cr-C-Ni powder mixture as the matrix to prepare a wear-resistant $(Cr, Fe)_7C_3$ carbide-reinforced composite coating on a 0.45% C carbon steel matrix by plasma transfer arc (PTA) surlaying process. The dry sliding wear test showed that $(Cr, Fe)_7C_3$ carbide composite coating has high hardness and excellent wear resistance. Ma et al. [10] mixed MoS_2 and graphite on the surface of iron-based powder metallurgy materials in a certain proportion to prepare a composite bonded lubrication coating. The end-face friction and wear test was conducted, and the results showed that when the

bonded coating had a higher proportion of graphite, the friction and wear characteristics were good. In addition, changing the surface wettability is another effective strategy; the better the surface wettability of the friction pair, the easier the liquid is to spread on the friction pair to form a lubricating layer so that the lubrication performance of the friction pair can be improved. Cottin-Bizonne et al. [11] believe that the microstructure of the material surface not only affects the contact angle and wettability of the material surface but also plays a role in surface friction, wear, lubrication, adhesion and other properties. Wen et al. [12] prepared micro-texture surface on 304 stainless steel surface by laser processing in air and anhydrous ethanol environment and found that texture morphology and surface chemical composition had major effects on the wettability of 304 stainless steel surface. Yadav et al. [13,14] used aluminum alloy 6061(AA6061) as the matrix material and alumina (Al_2O_3), aluminum nitride (AlN) and silicon carbide (SiC) as the reinforcement material to prepare two kinds of metal matrix composite materials. The tribological properties of the composites were tested by a pin-on-disc (POD) tribometer. The effects of composition, sliding velocity (SV), sliding distance (SD) and load on specific wear rate are studied. In addition, the erosion wear properties of alumina (Al_2O_3) and E-glass fiber-reinforced epoxy composites were studied, and it was proved that Al_2O_3 particles had strong interaction with polymer matrix and had good stress transfer properties. Cui et al. [15] studied the effects of CF/PEEK composites of different lengths on wettability and tribological properties and found that after adding carbon fiber, the friction coefficient and friction amount of CF/PEEK composites were reduced, and the wear resistance was enhanced, and the longer the fiber, the better the wear resistance. Since surface free energy is one of the main factors affecting the wettability of the friction pair surface [16], the use of a low surface energy modification method to prepare a hydrophobic surface is a way to improve the lubrication performance. Borruto et al. [17] selected 5 kinds of materials with different water contact angles to form friction pairs with different wetting combinations, respectively. Under the condition of water lubrication, tribological tests were conducted on these materials with a pin–disc tribometer. The research shows that the friction pair composed of a hydrophobic disc and hydrophilic pin can form a continuous water film between the disc and pin, which has a better lubrication effect and better friction and wear performance. Vengatesh et al. [18] successfully prepared the surface of self-lubricating superhydrophobic anodized aluminum oxide by electrochemical deposition coupled with low surface energy modification and conducted tribological tests using a pin–disc tribometer. The results show that the chemically grafted AAO nanostructures have higher seawater corrosion resistance and lower friction coefficient. Kuzina et al. [19] created hydrophobic coatings on tungsten and aluminum surfaces by using fluoroxysilane. Conradi et al. [20] prepared superhydrophobic surfaces by coating the textured surfaces with fluorinated SiO_2 nanoparticles and conducted experiments to explore the friction characteristics of different textured surfaces under two lubrication conditions: dry friction and water lubrication. With the increase in the surface roughness of coated SiO_2, the surface gradually changes from a hydrophobic surface to a superhydrophobic surface, and the friction coefficient becomes significantly smaller. Ou et al. [21] pointed out that the laminar flow of water through microchannels can be significantly reduced by using hydrophobic surfaces with well-defined surface roughness in the micron scale.

It can be seen that most studies on the improvement of friction performance by surface wettability focus on the direction of hydrophobic and superhydrophobic surfaces [22,23], but there is a lack of research on the improvement of friction performance by wettability under the condition of oil lubrication when materials modified with low surface energy are paired with each other. In this paper, SAF2507 duplex stainless steel and CFRPEEK were selected as matching materials to process the valve plate pair of an axial piston pump, and the low surface energy modification was carried out to improve its oil philicity. An MMD-5A friction and wear testing machine was used to investigate the friction and abrasion of different wettability combination valve plate pairs in the L-HM46# anti-wear hydraulic oil working environment.

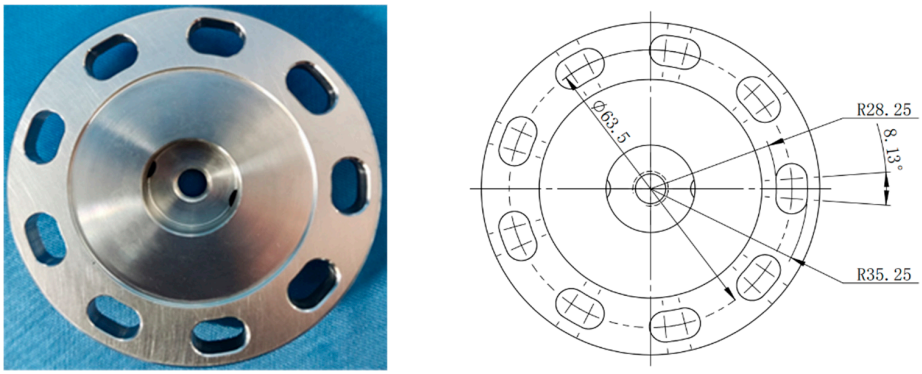
2. Materials and Methods

2.1. Sample Preparation

Super duplex stainless steel SAF2507 chromium and molybdenum content are very high, so it has excellent resistance to spot corrosion, uniform corrosion and crevice corrosion ability. The biphase microstructure also causes the steel to have high resistance to stress corrosion cracking.

Polyether ether ketone (PEEK) has the characteristics of high-temperature resistance, self-lubrication, wear resistance and fatigue resistance and has become one of the most popular high-performance engineering plastics at present. Carbon fiber-reinforced polyether ether ketone (CFRPEEK) further enhances the mechanical properties, thermal properties and tribological properties of PEEK, overcoming the disadvantages of ordinary thermoplastic resin materials such as low strength, low softening temperature and low elastic modulus.

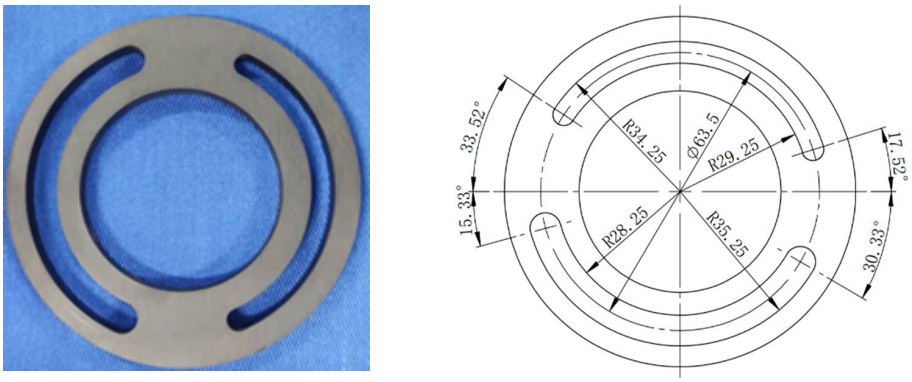
The lining plate of the duplex stainless steel SAF2507 cylinder block of the upper sample is the ring sample created by mechanical processing, the lower sample CFRPEEK valve plate is the disc sample created by CNC processing, and the upper and lower friction surface is smooth. As shown in Figure 1, the sample of a duplex stainless steel SAF2507 physical picture and processing size schematic diagram, the inner diameter of the friction surface of the sample is 50 mm, the outer diameter is 76 mm and the average diameter of the friction torus is 63.5 mm.



(**a**) (**b**)

Figure 1. Upper sample physical picture and processing size diagram. (**a**) Upper sample; (**b**) Upper sample size diagram.

As shown in Figure 2, the sample CFRPEEK physical picture and the schematic diagram of processing size, the friction surface of the sample under CFRPEEK has an outer diameter of Φ80 mm, an inner diameter of Φ46 mm and a thickness of 6 mm. There are two flow distribution windows on the friction surface.



(**a**) (**b**)

Figure 2. Lower sample physical picture and processing size diagram. (**a**) Lower sample; (**b**) Lower sample size diagram.

2.2. Preparation of Low Surface Energy Modified Sample

An amount of 0.5 mL of 1H,1H,2H, 2H-perfluoro-decyl trimethoxy-silane (PFOTES, 97%) was dissolved in 100 mL of anhydrous ethanol (analytically pure, 99.7%) and stirred with a glass rod until the liquid was uniformly transparent to obtain a low surface energy solution. The upper/lower samples were soaked in a low surface energy solution for 2 h and modified, and the samples were taken out and placed in a drying oven at 100 °C for 30 min to accelerate the reaction speed and make the hydrophobic structure on the surface of the samples more stable. After removal, the samples were cleaned with acetone and water, in turn, in the ultrasonic cleaning machine for 20 min, the excess molecular film on the surface was washed off, and the samples were air-dried. An up/down sample with low surface energy is prepared.

The modification mechanism of PFOTES on upper and lower samples was specifically analyzed as shown in Figure 3. The molecular formula of PFOTES is $C_{13}H_{13}F_{17}O_3Si$, which contains two main groups, -Si-OCF_3 and -F. -Si-OCF_3 can be used to link the molecule to the surface of the sample, so the -F group is correspondingly present on the surface of the sample to achieve surface modification. The molecular formula of PFOTES is $C_{13}H_{13}F_{17}O_3Si$. Its molecular terminal group -Si-OCF_3 will hydrolyze with a trace amount of water in an anhydrous ethanol solution to form the -Si-OH group, which will be dehydrated and condensed with the -OH group on the surface of the upper and lower samples to modify the long-chain silane molecules to the surface of the sample. The oleophobic molecules are cross-linked by heating in a drying oven [20].

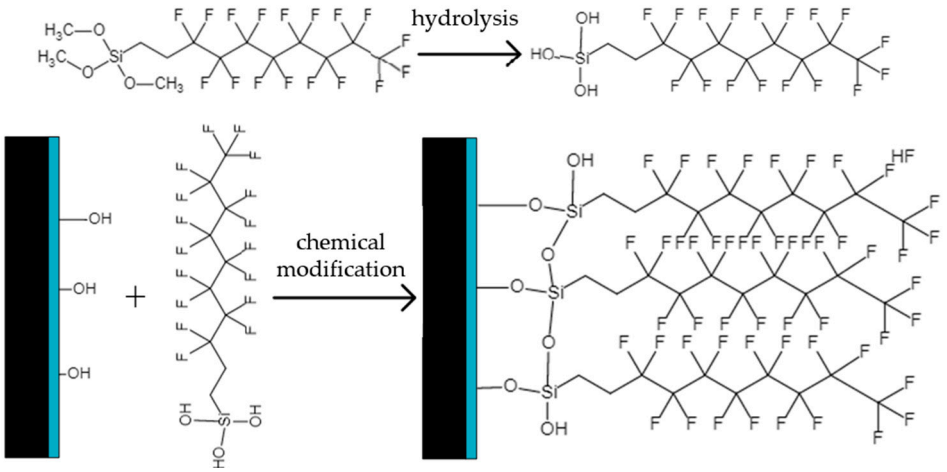


Figure 3. Modification mechanism of PFOTES on upper and lower samples.

After being held and dried at 100 °C for 30 min, relatively stable perfluoro methyl groups were formed on the surface of the sample, and the perfluoro methyl groups were hydrophobic, so the contact angle of the upper and lower samples after modification with low surface energy solution became significantly larger, and the surface became hydrophobic [24].

The UC-120D ultrasonic cleaning instrument is used to clean the upper and lower samples before and after the test. The electric thermostatic drying oven is used to prepare samples with low surface energy up and down, accelerate the reaction rate and make the hydrophobic structure on the surface of the sample more stable. The test temperature is set at 100 °C, and the holding time is 30 min.

2.3. Calculation of Surface Free Energy of the Sample

At present, the most widely used method for the calculation of surface free energy is the Owens two-liquid method, which calculates the surface free energy of a solid by measuring the different contact angles between the solid surface and the liquid with different surface tensions [25–27].

The intrinsic contact angle θ can be described by Young's equation [28]:

$$\gamma_{SV} = \gamma_{SL} + \gamma_{LV} cos\theta \quad (1)$$

where:

γ_{SL} is the surface tension between the solid–gas interface; γ_{LV} is the surface tension at the liquid–gas interface; γ_{SV} is the surface tension between the liquid–solid interface;

θ is the intrinsic contact angle of gas–liquid–solid three-phase equilibrium.

The surface free energy of a solid is the sum of the polar force γ^p and the dispersion force γ^d, namely:

$$\gamma = \gamma^p + \gamma^d, \quad (2)$$

If there are both dispersive and polar force interactions between solid and liquid, the solid–liquid interface free energy should be expressed as:

$$\gamma_{SL} = \gamma_{LV} + \gamma_S^0 - 2\sqrt{\gamma_S^d \gamma_{LV}^d} - 2\sqrt{\gamma_S^p \gamma_{LV}^p}, \quad (3)$$

where:

Superscript p represents the polar component of solid surface energy;

Superscript d represents the dispersion component of solid surface energy;

γ_S^0 represents the specific surface energy of a solid in a vacuum.

Substituting Young's Equation (1) into Equation (3), we obtain:

$$\gamma_{LV}(1 + \cos\theta) = 2\sqrt{\gamma_S^d \gamma_{LV}^d} + 2\sqrt{\gamma_S^p \gamma_{LV}^p}, \quad (4)$$

where:

γ_S^p and γ_S^d are the polar force and dispersion force of the free energy on the solid surface, respectively;

γ_{LV}^p and γ_{LV}^d are the polar force and dispersion force of the free energy at the liquid–gas interface, respectively.

There are only two unknowns, γ_S^p and γ_S^d, in the equation, and the surface free energy of the solid can be calculated by finding two liquids with known γ_{LV}^p and γ_{LV}^d and measuring their contact angles on the solid surface.

2.4. Measurement of Tribological Properties

The MMD-5A multifunctional friction and wear testing machine was used for the friction test. Figure 4 shows the friction and wear testing machine and its test installation diagram.



Figure 4. Friction and wear testing machine and specimen installation drawing.

2.5. Measurement of Contact Angle

In this paper, the HARKE-SPCAX1 contact angle tester produced by HARKE (Beijing, China) is used to measure the contact angle of the sample. The morphology of the droplet is analyzed by using the relevant software in the computer and combined with the theory of the Young–Laplace equation. The contact angle of the droplet on the surface of the sample is calculated. The morphology of the samples was analyzed by a ZEISS (Jena, Germany) Gemini SEM field emission scanning electron microscope.

2.6. Friction and Wear Test

Before the test, the samples to be used were cleaned with a UC-120D ultrasonic cleaning instrument and allowed to air-dry naturally. Some of the samples were used to prepare low surface energy samples, and the microscopic morphology of the upper and lower samples was observed by laser microscope. The HARKE-SPCAX1 contact angle tester was used to measure the surface contact angle of the upper and lower samples. The friction and wear test was carried out on an MMD-5A multifunctional standard friction and wear test machine under the condition of hydraulic oil lubrication. After the friction test was completed, the friction coefficient curve with time was obtained.

After the test, the sample was cleaned and dried, and the worn surface was observed. Finally, the friction and wear characteristics of axial piston pump valve plate pairs with different wetting combinations under hydraulic oil lubrication were analyzed by combining the data obtained after the test and comparing them with the data before the test.

In the friction and wear test, the normal load is set to 300 N, and the rated speed is 600 r/min, 800 r/min, 1000 r/min, and 1200 r/min, respectively. Since the center circle diameter of the friction torus of the valve plate pair is 63.5 mm, the friction and wear test in this paper adopts hydraulic oil lubrication. In past experience, the friction coefficient will reach a stable state around experiment 7200 s, and the friction coefficient curve is stable. The test time of each valve plate pair lasts for 7200 s, with a total of 16 groups of tests. The specific experimental scheme is shown in Table 1.

Table 1. Friction and wear test scheme.

Test Number	Friction Pair	Normal Force (N)	Test Time (s)
ULI	Upper and lower initial samples	300	7200
UILM	Upper initial sample—Lower modified sample	300	7200
UMLI	Upper modified sample—Lower initial sample	300	7200
ULM	Upper and lower modified samples	300	7200

3. Results

3.1. Energy Spectrum of SAF2507

The surface element composition of SAF2507 was measured by EDS, and the surface energy spectrum after coating is shown in Figure 5. Compared with the chemical composition of the original surface of SAF2507, as shown in Table 2, the contents of F and Si elements on the surface of the top sample after coating with low surface energy substances significantly increased due to the presence of perfluoromethyl groups, and the carbon content slightly increased.

Table 2. Chemical composition of duplex stainless steel SAF2507 (ω/%).

Element	C	Mn	Si	S	P	Cr	Ni	Mo	Cu	N
Content	≤0.03	≤1.20	≤0.8	≤0.02	≤0.035	24.0–26.0	6.0–8.0	3.0–5.0	≤0.5	0.24–0.32

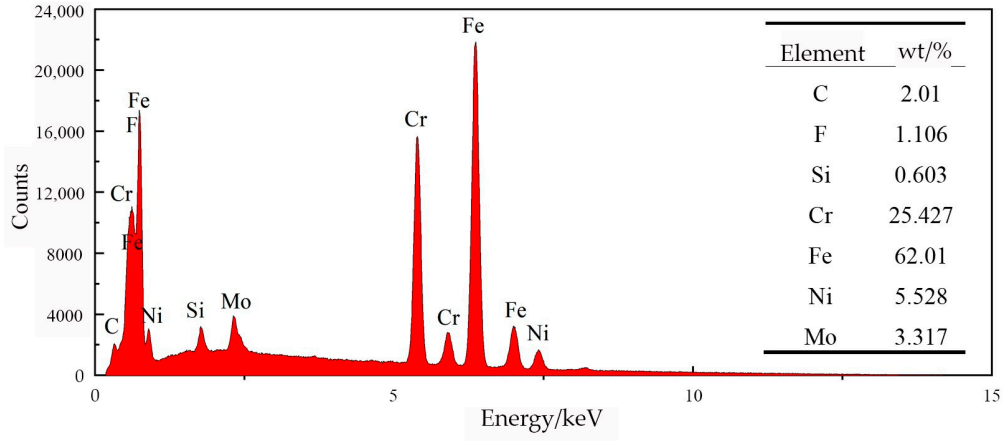


Figure 5. Surface energy spectrum of SAF2507 after coating.

3.2. Sample Surface Free Energy

In this paper, the Owens two-liquid method was used to measure the surface free energy of the initial and modified samples above and below by using the different contact angles between polar liquid water and nonpolar liquid n-cetane and the samples. The surface free energy of water and n-cetane is shown in Table 3.

Table 3. Measuring surface free energy of liquid (mJ/m^2).

Liquid	γ_{LV}	γ_{LV}^{d}	γ_{LV}^{P}	$\gamma_{LV}^{P}/\gamma_{LV}^{d}$	**Polarity**
water	72.8	21.8	51.0	2.36	polar
n-cetane	27.6	27.6	0	0	nonpolar

The polar force γ_S^p, dispersion force γ_S^d and total surface free energy γ_S of the initial and modified samples were calculated by substituting the measured contact angles of water and n-hexadecane on the upper and lower initial samples and the modified samples by Equation (4), as shown in Figure 6.

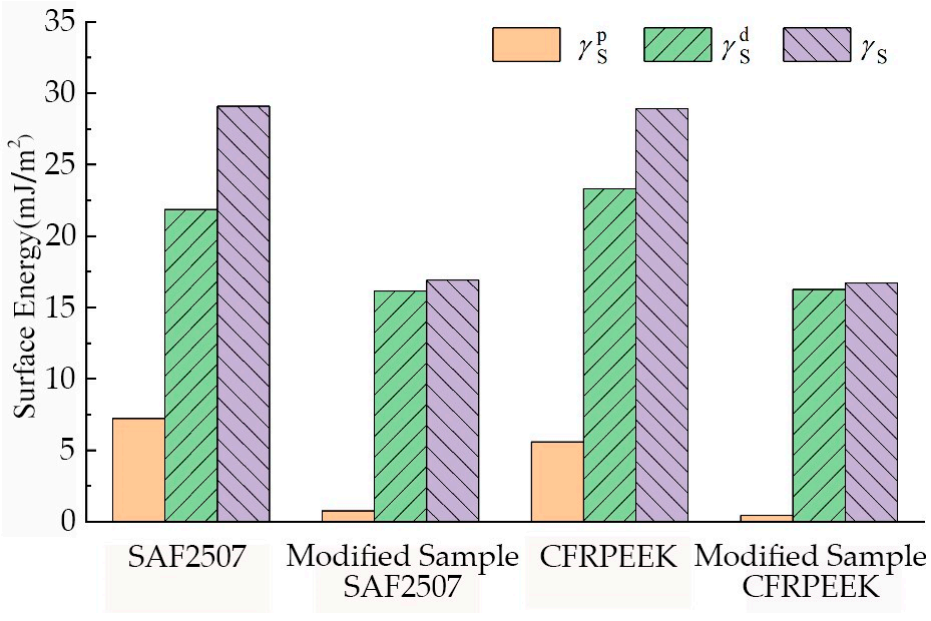


Figure 6. Surface energy of initial and modified samples.

After coating the low surface energy solution, the surface free energy of the upper and lower samples decreased from 29.08 mJ/m^2 and 28.92 mJ/m^2 to 16.91 mJ/m^2 and 16.71 mJ/m^2, respectively. The polar force decreased from 7.23 mJ/m^2 and 5.60 mJ/m^2 to 0.76 mJ/m^2 and 0.43 mJ/m^2, respectively. The dispersion force decreased from 21.85 mJ/m^2 and 23.33 mJ/m^2 to 16.28 mJ/m^2 and 16.15 mJ/m^2, respectively. The coating of low surface energy solution greatly reduces the polar force and dispersion force of the surface, and the surface free energy of the sample decreases.

3.3. Surface Wettability

It is a dynamic process from contact to wetting of the surface of the upper and lower samples. With time, droplets are constantly spreading, and the contact angle of the sample surface is also constantly changing. The hydraulic oil droplet with a volume of 1 μL was taken as the research object, the measurement time was 300 s and the ambient temperature was 20 °C. Figure 7 shows the change in the solid–liquid contact angle with time on the original surface (SAF2507 and CFRPEEK) and the low surface energy surface (modified sample) of the hydraulic oil liquid medium.

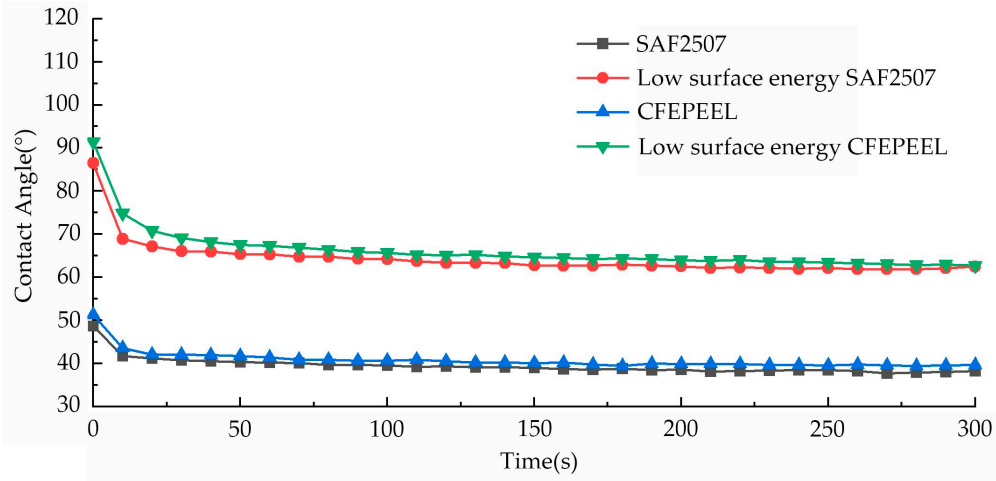


Figure 7. L-HM46# anti-wear hydraulic oil contact angle change with time within 300 s.

After 300 s of dripping oil, the oil contact angle quickly stabilized. The oil contact angles of SAF2507 and CFRPEEK are 38.7° and 45.4°, respectively. The oil contact angles of low surface energy SAF2507 and low surface energy CFRPEEK are 63.7° and 62.7°, respectively.

The entire process after the liquid drops onto the solid surface is analyzed, as shown in Figures 8–11.

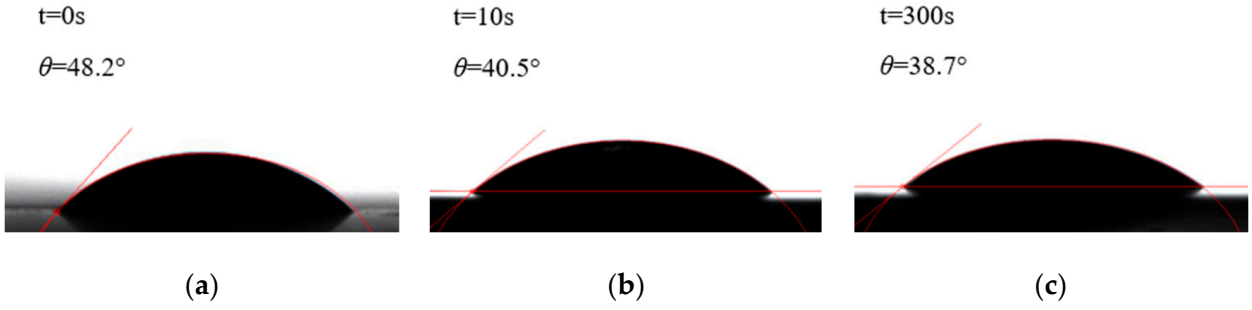


Figure 8. Droplet spreading diagram of SAF2507. (**a**) Initial contact angle; (**b**) Process contact angle; (**c**) Equilibrium contact angle.

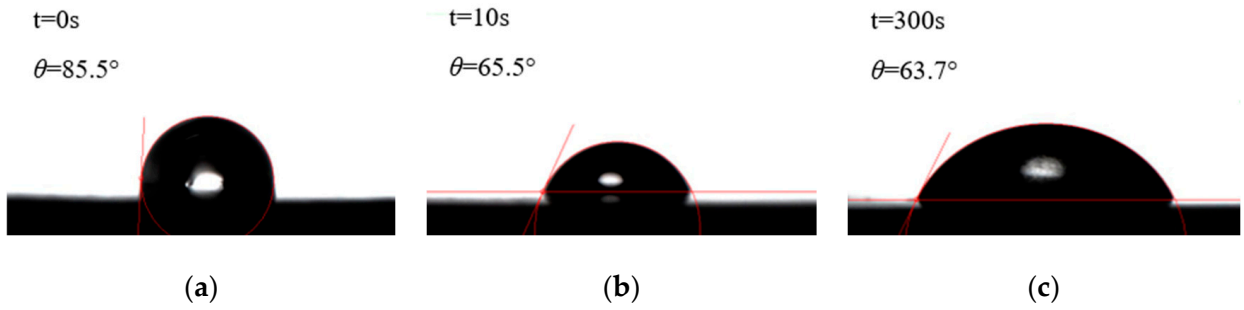


Figure 9. Droplet spreading diagram of low surface energy SAF2507. (**a**) Initial contact angle; (**b**) Process contact angle; (**c**) Equilibrium contact angle.

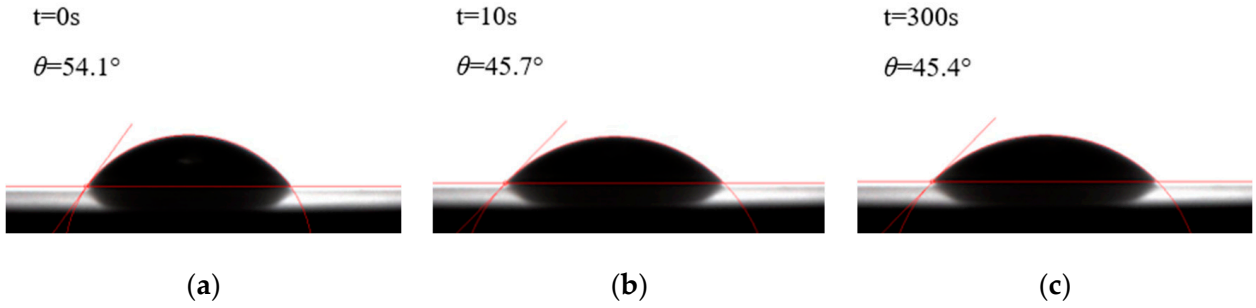


Figure 10. Droplet spreading diagram of CFEPEEK. (**a**) Initial contact angle; (**b**) Process contact angle; (**c**) Equilibrium contact angle.

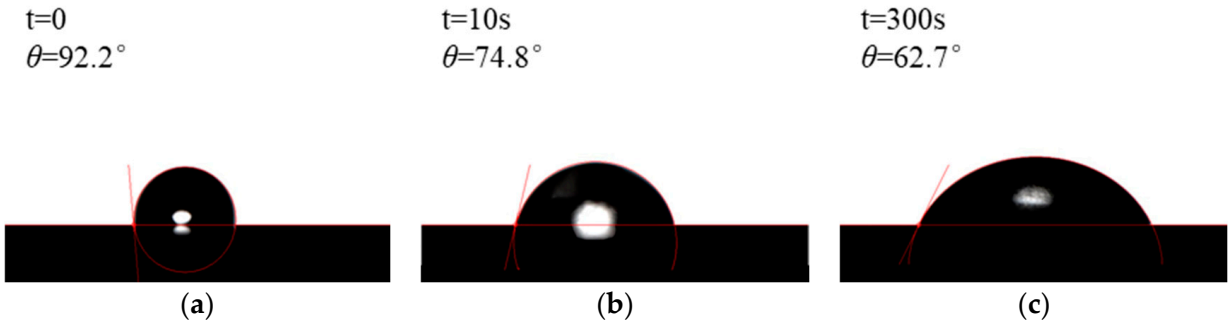


Figure 11. Droplet spreading diagram of low surface energy CFEPEEK. (**a**) Initial contact angle; (**b**) Process contact angle; (**c**) Equilibrium contact angle.

The liquid drops on the low surface energy CFEPEEK surface can be divided into three stages. The first stage: within 0–2 s after the measured liquid at the needle of the liquid injector is just in contact with the measured solid surface and leaves the needle, different initial contact angles will be formed due to the different types of the measured liquid, and their size mainly depends on the liquid–solid interface energy. The second stage: within 2~60 s of the initial contact angle formation, the energy of the system formed by the liquid and solid surface is in an unbalanced state, and the liquid rapidly spreads and infiltrates under the comprehensive effect of its own gravity, intermolecular forces, liquid surface tension and the capillary effect of the rough surface of solid on liquid, so that the solid–liquid contact angle decreases continuously, as shown in Figure 8b. The third stage: within 60~300 s, the energy of the whole system tends to be stable, the driving effect of the liquid heavy force gradually weakens, the downward pressure generated by the surface tension of the spherical liquid continuously decreases, the spreading speed of the liquid gradually slows down. After 300 s, it finally stabilizes at a fixed value, that is, the equilibrium contact angle, as shown in Figure 8c.

3.4. Friction Coefficient

Figures 12–15 show the change curves of friction coefficients of different oil-wet surface combination valve pairs with time under hydraulic oil lubrication at rated speeds of 600 r/min, 800 r/min, 1000 r/min, and 1200 r/min, respectively.

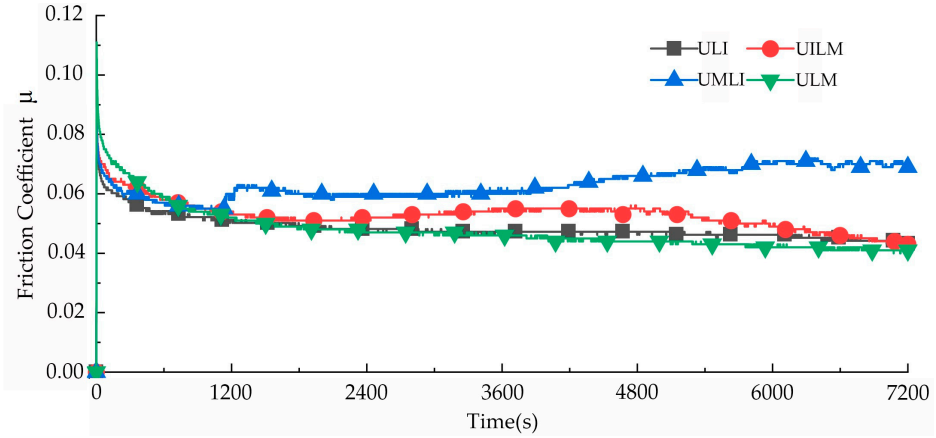


Figure 12. Change curve of friction coefficient of valve plate pairs with different oil-wet surfaces under 600 r/min hydraulic oil lubrication with time.

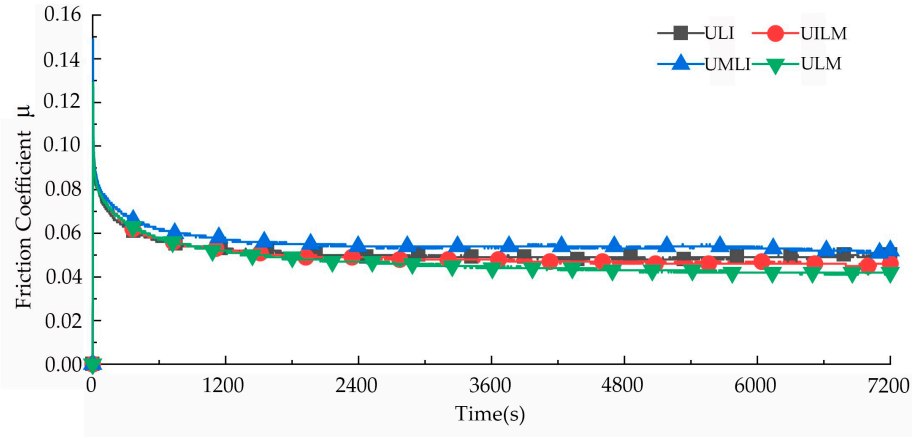


Figure 13. Change curve of friction coefficient of valve plate pairs with different oil-wet surfaces under 800 r/min hydraulic oil lubrication with time.

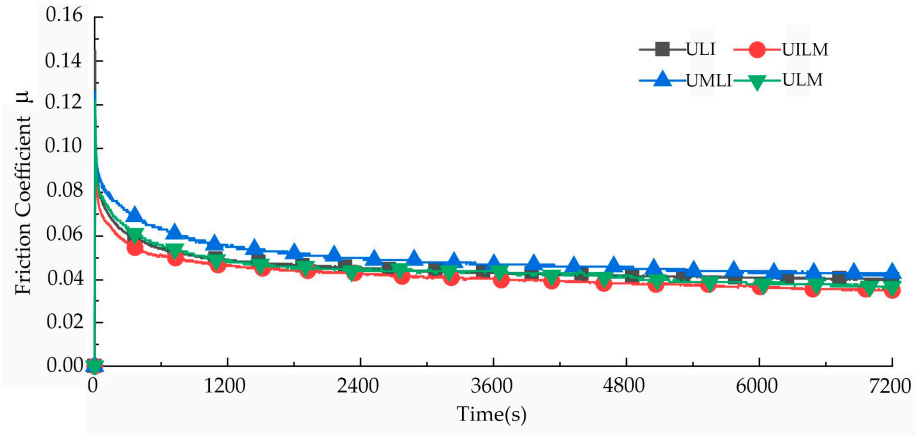


Figure 14. Change curve of friction coefficient of valve plate pairs with different oil-wet surfaces under 1000 r/min hydraulic oil lubrication with time.

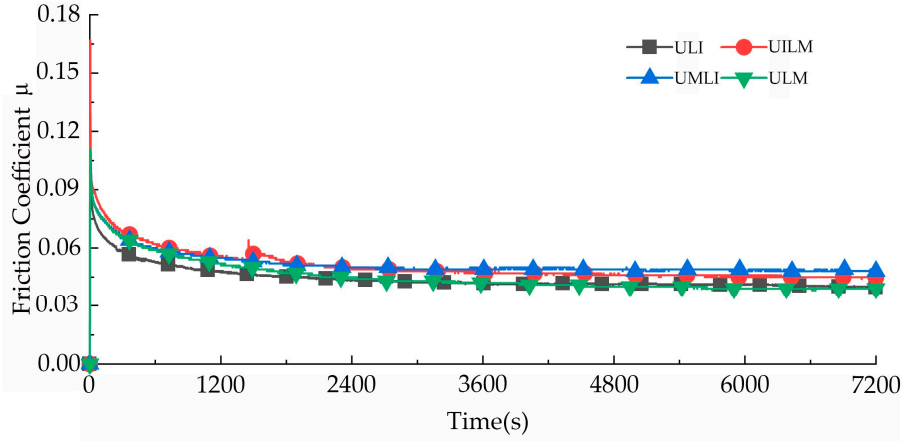


Figure 15. Change curve of friction coefficient of valve plate pairs with different oil-wet surfaces under 1200 r/min hydraulic oil lubrication with time.

Observation of Figure 12 shows that in the rated speed of 600 r/min under the working conditions of hydraulic oil lubrication, the friction coefficient of the distribution pair of group ULI rapidly decreases from 0.087 at the beginning to 0.054 within 600 s of the initial test, and then the decline rate of the friction coefficient slows down. After 2200 s of the test, the friction coefficient gradually stabilized at about 0.048, and at the end of the test, the friction coefficient stabilized at about 0.046. In the 600 s after the test, the friction coefficient of the UIML and UMLI pairs decreased from 0.089 and 0.088 to 0.058, respectively. In the later test time, the friction coefficient of the UIML pairs gradually decreased to about 0.044 after a slow rise, while the friction coefficient of the UMLI pairs slowly climbed to about 0.07 with the progress of the test. The friction coefficient of the two groups is slightly higher than that of group ULI. The friction coefficient of the distribution pair of group ULM was slightly higher than that of group ULI in the first 1480 s of the test, and lower than that of group ULI after 1480 s, and finally stabilized at 0.041.

Observation of Figure 13 shows that under the working condition of hydraulic oil lubrication at a rated speed of 800 r/min, the friction coefficient of the four combinations of valve plate pairs decreases rapidly from 0.1~0.14 to 0.058~0.061 within the first 600 s of the test. With the progress of the friction test, the friction coefficient decreases slowly and gradually tends to be stable. The friction coefficients of ULI, UILM, UMLI and ULM were finally stabilized at 0.049, 0.046, 0.052 and 0.042, respectively.

According to Figures 14 and 15, it can be seen that under the working conditions of hydraulic oil lubrication with a rated speed of 1000 r/min and 1200 r/min, the friction coefficient curves of each valve plate pair have similar trends to those of each valve plate pair with a rated speed of 800 r/min. Specific analysis shows that the friction coefficients of ULI, UILM, UMLI and ULM are stabilized at 0.04, 0.035, 0.037 and 0.042, respectively, under the rated speed of 1000 r/min. When the rated speed is 1200 r/min, the friction coefficient of the valve plate pair of group ULI is stable at about 0.04. The friction coefficient of groups UILM and UMLI is always slightly higher than that of group ULI, and their friction coefficient is stable at about 0.048 and 0.045, respectively. Before 3600 s, the friction coefficient of group ULM is slightly higher than that of group ULI, but gradually lower than that of group ULI after 3600 s, and the friction coefficient is stable at about 0.039 at the end of the test.

The average friction coefficient of each pair and the speed of the sample were taken to create a scatter plot, and the relationship between them was linearly fitted. The linear fitting curve is shown in Figure 16. With the increase in rotational speed, the average friction coefficient of all pairs showed a downward trend, and the UMLI pair dropped the most, while the ULM pair always maintained a low friction coefficient. When the speed increases gradually, the lubrication effect of the four pairs tends to be consistent.

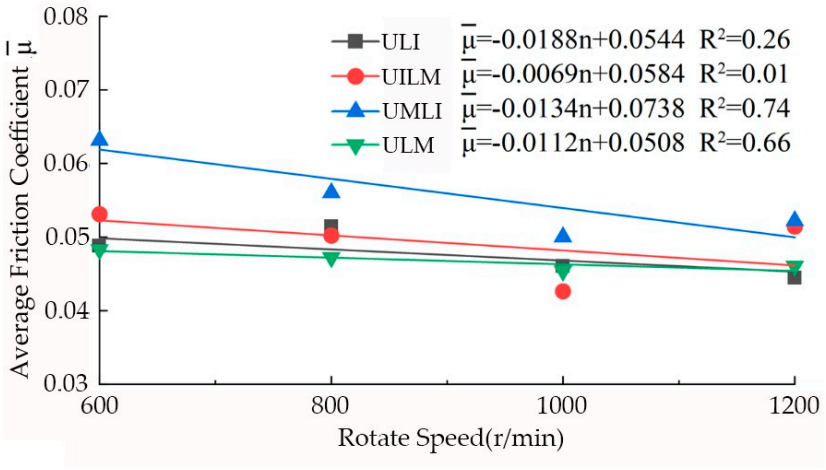


Figure 16. Linear fitting curves of average friction coefficients of combined valve pairs with different oil-wet surfaces under hydraulic oil lubrication.

3.5. Wear Surface and Frictional Wear Characteristics

The surface wear morphologies of the samples were observed under a microscope. The macro wear surfaces of the upper and lower samples and the 2D and 3D microscopic wear morphologies of the four different wetting pairs under the working conditions of hydraulic oil lubrication with normal force P = 300 N and rotational speed n = 1200 r/min are shown in Figures 17–20.

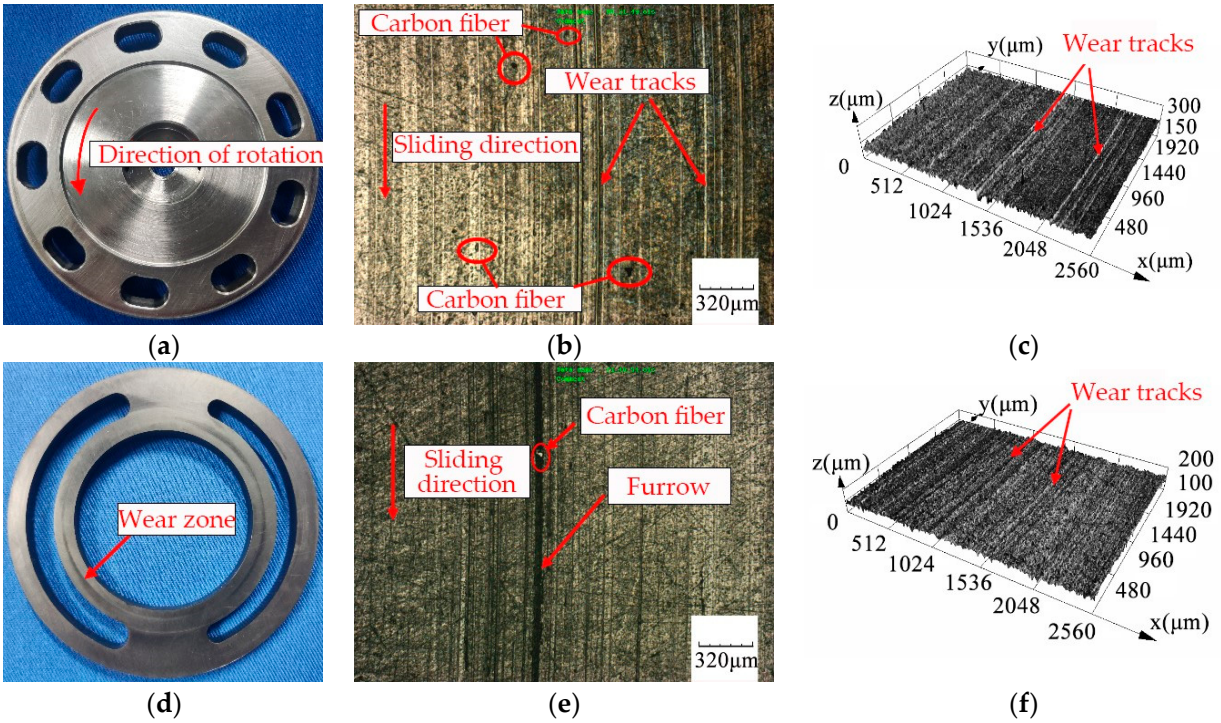


Figure 17. Group ULI specimen wear diagram. (**a**) Macroscopic diagram of upper sample; (**b**) Microscopic two-dimensional diagram of upper sample; (**c**) Microcosmic three-dimensional diagram of upper sample; (**d**) Macroscopic diagram of lower sample; (**e**) Microscopic two-dimensional diagram of lower sample; (**f**) Microcosmic three-dimensional diagram of lower sample.

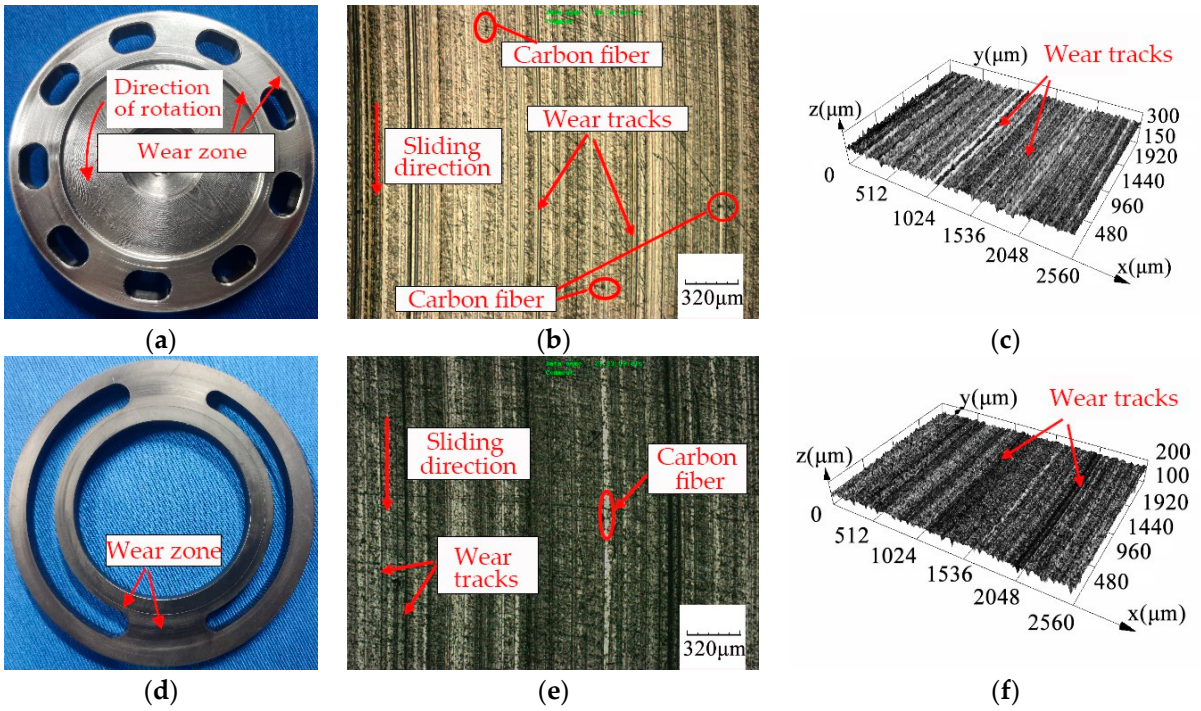


Figure 18. Group UILM specimen wear diagram. (**a**) Macroscopic diagram of the upper sample; (**b**) Microscopic two-dimensional diagram of the upper sample; (**c**) Microcosmic three-dimensional diagram of the upper sample; (**d**) Macroscopic diagram of the lower sample; (**e**) Microscopic two-dimensional diagram of the lower sample; (**f**) Microcosmic three-dimensional diagram of the lower sample.

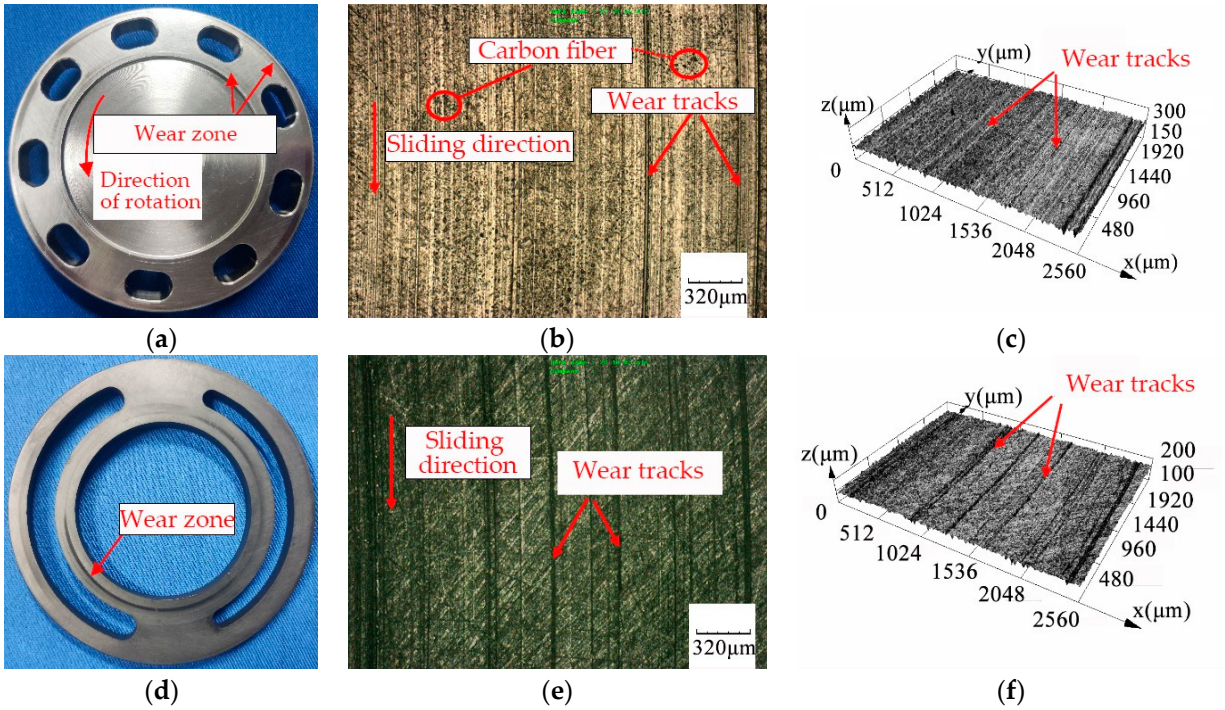


Figure 19. Group UMLI specimen wear diagram. (**a**) Macroscopic diagram of the upper sample; (**b**) Microscopic two-dimensional diagram of the upper sample; (**c**) Microcosmic three-dimensional diagram of the upper sample; (**d**) Macroscopic diagram of the lower sample; (**e**) Microscopic two-dimensional diagram of the lower sample; (**f**) Microcosmic three-dimensional diagram of the lower sample.

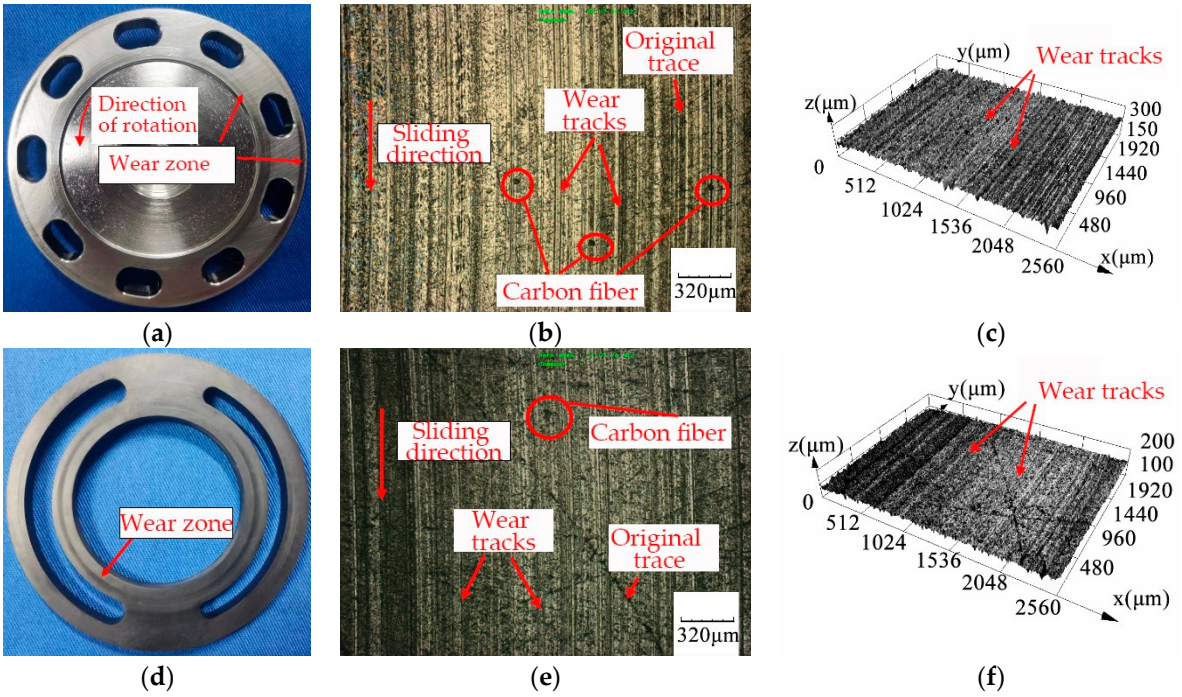


Figure 20. Group ULM specimen wear diagram. (**a**) Macroscopic diagram of the upper sample; (**b**) Microscopic two-dimensional diagram of the upper sample; (**c**) Microcosmic three-dimensional diagram of the upper sample; (**d**) Macroscopic diagram of the lower sample; (**e**) Microscopic two-dimensional diagram of the lower sample; (**f**) Microcosmic three-dimensional diagram of the lower sample.

From a macro point of view, narrow or wide wear bands appear on each valve plate pair, and the formation of wear bands is caused by periodic wear during the rotation of the upper sample SAF2507 around the central axis relative to the lower sample CFRPEEK.

Observing the flow of equipping vice sample after wear and tear on the micro 2D and 3D figures, the experiment before when sanding traces still exist, the sliding direction produced more grinding cracks, surface morphology was severely damaged; this is a "naked" in the next sample CFRPEEK surface as well as the "free" in the flow pair clearance of carbon fiber on the sample stainless steel cutting action.

By observing the microscopic 2D and 3D maps of the samples under each distribution pair after wear, it can be seen that similar to the samples above, the sandpaper wear tracks before the test still exist, and there are more wear marks on the surface of the sample in its sliding direction, but the furrow wear marks of the sample below are more dense, and the surface topography damage is more serious. The reason for this phenomenon is that the hardness of the duplex stainless steel SAF2507 on the upper sample is very large, and the rough peak on the surface is similar to a "plow" that repeatedly cultivates the surface of the lower sample during the rotation process, forming a clear furrow along the sliding direction.

During the friction process, under the "cutting" of the stainless steel rough micro-peak, a part of carbon fiber (CF) is exposed to the surface of CFRPEEK, a part of CF is crushed and pulled out, and then "free" to the valve plate pair; because the strength of CF is very high, the "free" CF plays an abrasive role on the stainless steel, thus aggravating the wear of stainless steel.

The wear depth was observed and analyzed under a 5× lens of an Olympus laser confocal microscope. Figure 21 shows the average wear depth of upper and lower samples after wear of different oil-wet surface combination valve plate pairs at different rotational speeds.

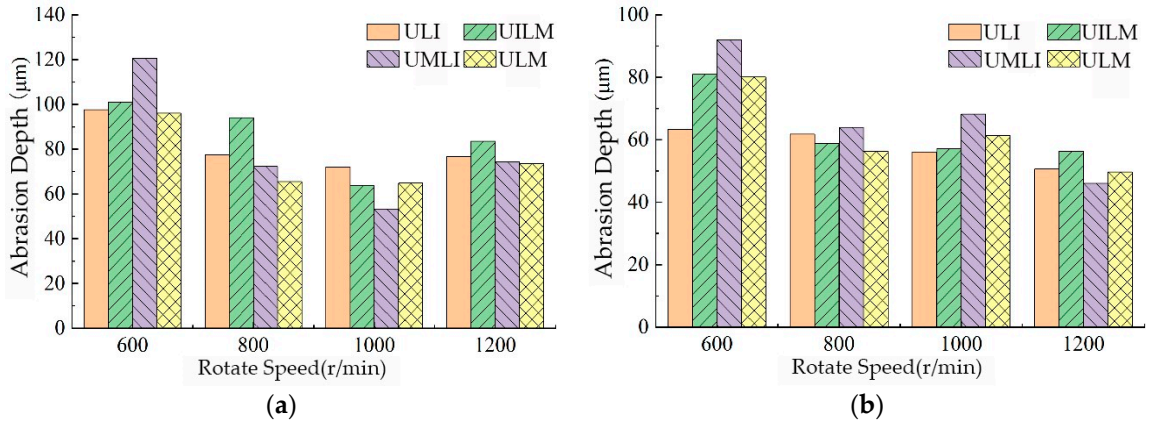


Figure 21. The depth of surface wear after different oil-wet surface combination valve plate pair wear. (**a**) Depth of abrasion on the surface of the upper sample; (**b**) Depth of abrasion on the surface of the lower sample.

Observation of Figure 21 shows that under the hydraulic oil lubrication conditions, with the increase in rotational speed, the flow of equipping the vice grinding crack depth basic has varying degrees of decline; in group (a), for example, the upper sample values in the rotational speed of the grinding crack depth were 97.68 μm, 77.48 μm, 72 μm and 76.8 μm. The wear depth values of the lower samples under different rotational speeds were 63.36 μm, 61.8 μm, 56.08 μm and 50.6 μm, respectively. Moreover, with the increase in speed, the difference between the valve plate pairs is less obvious, that is, the wettability has less influence on wear at high speed.

4. Discussion

Under the rotating speed of 1200 r/min, SAF2507 of the ULM group was used for EDS analysis of the wear surface, and its EDS energy spectrum is shown in Figure 22. CFRPEEK of the ULM group was used for EDS analysis of wear surface, and its EDS spectra are shown in Figure 23. The mass fraction of C element on the wear surface of SAF2507 is 8.8%, which should be derived from carbon fiber in the sample CFRPEEK. The energy spectrum of the worn surface of the lower sample CFRPEEK shows that 8.2% Fe element appears on the surface of the lower sample after wear, and this element transfer phenomenon confirms the existence of adhesive wear in the friction process.

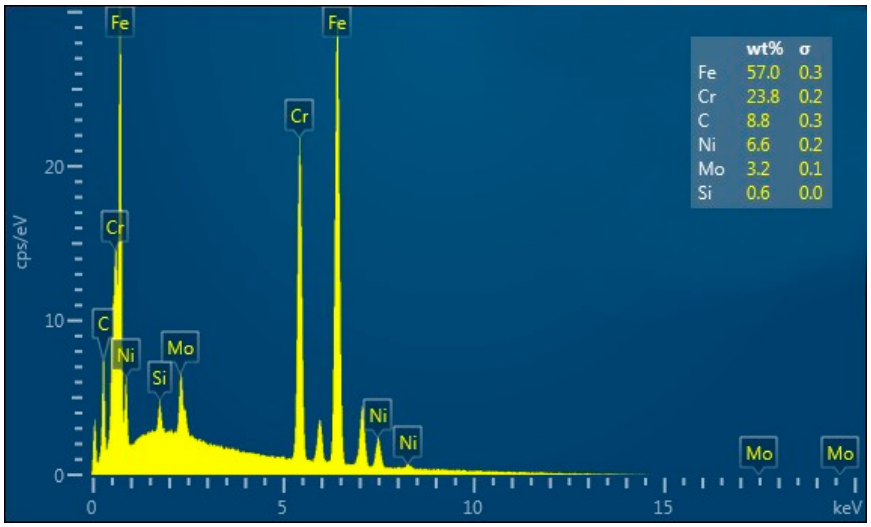


Figure 22. EDS energy spectrum of worn surface elements of SAF2507 in the ULM group.

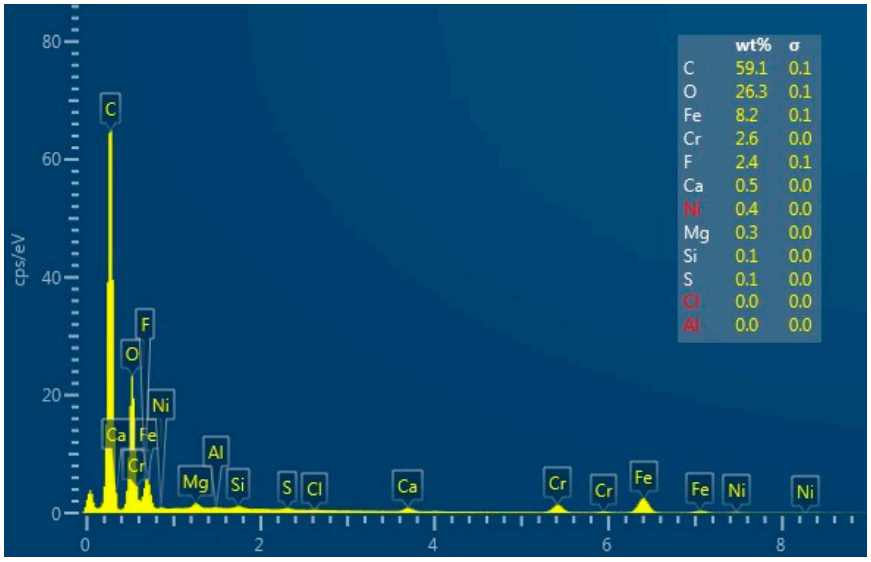


Figure 23. EDS energy spectrum of worn surface elements of CFRPEEK in the ULM group.

Comprehensive analysis of friction and wear process. Part of the wear chips produced in the run-in period are discharged from the friction surface with the hydraulic oil, and part of the wear chips are embedded into the softer lower sample CFRPEEK under pressure, participating in the subsequent wear and adhesive wear. Friction occurs on the upper and lower surfaces. In the process of contact between the micro-convex bodies on the upper and lower surfaces, the force of atoms and molecules will cause adhesion at the contact points. When the friction force generated in the process of relative sliding is greater than the adhesion between the micro-convex bodies, the low-strength CFRPEEK micro-convex bodies will be subjected to shear force and will be sheared away from the surface of the lower sample. With adhesion to the stronger SAF2507 micro-convex body, that is, adhesive wear occurs.

Under the condition of hydraulic oil lubrication, the friction between the upper and lower samples is mainly caused by the friction between the solid–liquid interface and the friction inside the lubricating oil [29]. The medium used in this paper is the same hydraulic oil, so the viscosity of the lubricating medium is certain, and the friction force inside the lubricating oil is unchanged at the same speed. At this time, the friction force between the upper and lower samples mainly depends on the friction force between the solid and liquid interface, and the friction force between the solid and liquid interface has a great relationship with the free energy of the solid surface. The original surface of the upper and lower samples has a strong residual chemical bond, and a large surface free energy can adsorb oil molecules firmly on its surface, resulting in a large adhesion between the interfaces. However, samples with low surface energy have low surface free energy, which can be obtained from the wall slip theory, and surfaces with strong oil-phobic properties are conducive to boundary slip [30]. Due to the velocity slip between the solid and liquid interface, the friction between the solid and liquid interface is greatly reduced, so there is a significant friction-reducing effect between the valve plate pairs on the weak oil-wet surface at the same speed. At high rotational speed, the spindle drives the upper sample to rotate rapidly and the upper sample to stir the lubricating oil to rotate faster. With the gradual increase in temperature, the viscous force of the oil decreases, and the friction inside the oil decreases, so the friction coefficient is small at high rotational speed. At high rotational speed, part of the oil forming the lubricating film will also slip outward under the action of centrifugal force, and the solid–liquid friction between the surface with low surface energy and the original surface tends to be consistent, so the friction coefficients of the four kinds of valve plate pairs tend to be consistent at high rotational speed.

5. Conclusions

In this paper, the valve plate pairs of axial piston pumps are taken as the research object. Fluorosilane was used to modify the upper and lower samples, and the solid–liquid contact angle was used as the index to characterize the surface wettability. The influence of the low surface energy modification method on the surface wettability of the valve plate pairs was investigated, and the tribological and wear properties of the SAF2507–CFRPEEK friction pair with different wetting combinations were investigated under different working conditions in the oil lubrication medium. The main conclusions of this paper are as follows:

(1) The coating of low surface energy solution greatly reduces the polar force and dispersion force of the surface, and the surface free energy of the sample is obviously reduced. The surface free energy of the upper and lower samples decreased by 41.9% and 42.2%, respectively.

(2) SAF2507 and CFRPEEK remained lipophilic after treatment with a low surface energy solution, but the oil contact angle was significantly enlarged. The spreading speed of the sample modified by low surface energy is lower than that of the original sample.

(3) Under the condition of hydraulic oil lubrication, under the condition of a low speed (800 r/min), the surface wettability of the valve plate pair has a great influence on its friction and wear characteristics, and the friction coefficient of the upper and lower modified samples decreases by 14.3% compared with that of the unmodified sample; Under the working condition of high speed (1200 r/min), the surface wettability of the valve plate pair has no significant influence on its friction and wear characteristics, and the difference in the friction and wear characteristics of the four valve plate pairs is not significant

(4) The friction process of SAF2507–CFRPEEK under the condition of hydraulic oil lubrication is mainly dominated by furrowing effects and adhesive wear.

Author Contributions: Conceptualization, Y.L. and D.G.; methodology, Y.L.; validation, W.W. and M.S.; formal analysis, W.W., H.X. and C.W.; investigation, Z.Z. and H.X.; resources, Y.L.; data curation, W.W.; writing—original draft preparation, Y.L., W.W. and M.S.; writing—review and editing, D.G., Z.Z. and C.W.; supervision, D.G.; project administration, Y.L.; funding acquisition, Y.L. and D.G. All authors have read and agreed to the published version of the manuscript.

Funding: This research was supported by the National Natural Science Foundation of China (Grant No. 52005428), the Hebei Natural Science Foundation (Grant No. E2020203107 and Grant No. E2021203099) and the Open Fund Project of Shaanxi Provincial Key Laboratory of Hydraulic Technology (No. YYJS2022KF04).

Institutional Review Board Statement: Not applicable.

Informed Consent Statement: Not applicable.

Data Availability Statement: All data generated or analyzed during this study are included in this article.

Conflicts of Interest: The authors declare no conflicts of interest.

References

1. Chao, Q.; Zhang, J.; Xu, B.; Huang, H.; Zhai, J. Centrifugal effects on cavitation in the cylinder chambers for high-speed axial piston pumps. *Meccanica* **2019**, *54*, 815–829. [CrossRef]
2. Liu, Y.S.; Wu, D.F.; Li, D.L.; Deng, Y.P. Applications and Research Progress of Hydraulic Technology in Deep Sea. *J. Mech. Eng.* **2018**, *54*, 14–23. [CrossRef]
3. Li, Y.L.; He, Y.Y.; Lou, J.B. Surface modifications and performance enhancements of key friction pairs in aviation hydraulic piston pumps. *J. Tsinghua Univ. (Sci. Technol.)* **2021**, *61*, 1405–1422.
4. Arup, M.; Chanchal, B.; Arghya, M.; Manoj, B.; Sathi, B. Comparative study of wear characteristics of selected structural materials. *Mater. Today Proc.* **2022**, *67*, 536–542.
5. Guo, X.T.; Xing, T.; Rang, J. Engineering Application and latest progress of Water Hydraulic Technology. *Chin. High Technol. Lett.* **2020**, *30*, 644–654.

6. Yang, D.Y.; Li, W.T.; Li, Z.Y. Present Situation and Forecating of Friction Pairs for High Pressure Piston Pump. *Hydraul. Pneum. Seals* **2022**, *42*, 1–7.
7. Chen, Y.L.; Ban, C.Z.; Liu, Y.S. Wear Model and Life Prediction of Port Pair in Aircraft Piston Pump. *Hydraul. Pneum.* **2020**, *12*, 1–7. [CrossRef]
8. Chen, W.; Liu, X.; Wen, H.X. Tribology and Prospect of PEEK Composites in Marine Environment. *Eng. Plast. Appl.* **2017**, *45*, 135–147.
9. Liu, Y.F.; Xia, Z.Y.; Han, J.M.; Zhang, G.L.; Yang, S.Z. Microstructure and wear behavior of (Cr, Fe)7C3 reinforced composite coating produced by plasma transferred arc weld-surfacing process. *Surf. Coat. Technol.* **2006**, *201*, 863–867. [CrossRef]
10. Ma, S.B.; Yi, Y.G.; Jiao, M.H. Study on the Tribological Properties of Adhesive Solid Lubricating Coating on Iron-based Materials. *Lubr. Eng.* **2008**, *33*, 36–39.
11. Cottin-Bizonne, C.; Barrat, J.L.; Bocquet, L. Low-friction Flows of Liquid at Nanopatterned Interfaces. *Nat. Mater.* **2003**, *2*, 237–240. [CrossRef]
12. Wen, Y.M.; Zhao, X.Y.; Wang, G.S. Wettability of Textured Surface of 304 Stainless Steel Prepared by One Step Method in Air/LiquidEnvironment. *China Surf. Eng.* **2021**, *34*, 97–103.
13. Yadav, R.; Meena, A.; Lee, S.Y. Experimental tribological and mechanical behavior of aluminium alloy 6061 composites incorporated ceramic particulates using Taguchi analysis. *Tribol. Int.* **2024**, *192*, 109243. [CrossRef]
14. Yadav, R.; Lee, H.H.; Meena, A. Effect of alumina particulate and E-glass fiber reinforced epoxy composite on erosion wear behavior using Taguchi orthogonal array. *Tribol. Int.* **2022**, *175*, 107860. [CrossRef]
15. Cui, X.H.; Li, Y.; Liu, X.Q. Study on wettability and tribological properties of PEEK composite reinforced by CF with different lengths. *New Chem. Mater.* **2020**, *48*, 146–149.
16. Liu, S.H.; Luo, J.B.; Li, G. Effect of Surface Physicochemical Properties on the Lubricating Properties of Water Film. *Appl. Surf. Sci.* **2008**, *251*, 7137–7142. [CrossRef]
17. Borruto, A.; Crivellone, G.; Marani, F. Influence of Surface Wettability on Friction and Wear Tests. *Wear* **1998**, *222*, 57–65. [CrossRef]
18. Vengatesh, P.; Kulandainathan, M.A. Hierarchically Ordered Self-Lubricating Superhydrophobic Anodized Aluminum Surfaces with Enhanced Corrosion Resistance. *ACS Appl. Mater. Interfaces* **2015**, *7*, 1516–1526. [CrossRef] [PubMed]
19. Kuzina, E.A.; Omran, F.S.; Emelyanenko, A.M. On the Significance of Selecting Hydrophobization Conditions for Obtaining Stable Super-hydrophobic Coatings. *Colloid J.* **2023**, *85*, 59–65. [CrossRef]
20. Conradi, M.; Drnovšek, A.; Gregorčič, P. Wettability and Friction Control of a Stainless Steel Surface by Combining Nanosecond Laser Texturing and Adsorption of Superhydrophobic Nanosilica Particles. *Sci. Rep.* **2018**, *8*, 7457. [CrossRef]
21. Ou, J.; Perot, J.B.; Rothstein, J. Laminar drag reduction in microchannels using ultrahydrophobic surfaces. *Phys. Fluids* **2004**, *16*, 4635–4643. [CrossRef]
22. Wen, L.P.; Tian, Y.; Jiang, L. Bioinspired Super-Wettability from Fundamental Research to Practical Applications. *Angew. Chem. Int. Ed.* **2015**, *54*, 3387–3399. [CrossRef]
23. Qin, L.G.; Lin, P.; Zhang, Y.L.; Dong, G.N.; Zeng, Q.F. Influence of Surface Wettability on the Tribological Properties of Laser Textured Co–Cr–Mo Alloy in Aqueous Bovine Serum Albumin Solution. *Appl. Surf. Sci.* **2013**, *268*, 79–86. [CrossRef]
24. Song, X.Y.; Zhai, J.; Wang, Y.L. Fabrication of Superhydrophobic Surfaces by Self-Assembly and Their Water-Adhesion Properties. *J. Phys. Chem. B* **2005**, *109*, 4048–4052. [CrossRef]
25. Barshilia, H.C.; Mohan, D.K.; Selvakumar, N. Effect of Substrate Roughness on the Apparent Surface Free Energy of Sputter Deposited Superhydrophobic Polytetrafluoroethylene Thin Films. *Appl. Phys. Lett.* **2009**, *95*, 33116. [CrossRef]
26. Razi, S.; Mollabashi, M.; Madanipour, K. Laser Processing of Metallic Biomaterials: An Approach for Surface Patterning and Wettability Control. *Eur. Phys. J. Plus* **2015**, *130*, 12. [CrossRef]
27. Rudawska, A.; Jacniacka, E. Analysis for determining surface free energy uncertainty by the Owen–Wendt method. *Int. J. Adhes. Adhes.* **2009**, *29*, 451–457. [CrossRef]
28. Young, T. Experiments and Calculations Relative to Physical Optics. *Philos. Trans. R. Soc. A* **1804**, *94*, 1–16.
29. Yoshimitsu, T.; Nakajima, H.; Nagaoka, H. Synthesis of the CD Ring System of Paclitaxel by Atom-transfer Radical Annulation Reaction. *Tetrahedron Lett.* **2002**, *43*, 8587–8590. [CrossRef]
30. Kunert, C.; Harting, J. Simulation of Fluid Flow in Hydrophobic Rough Microchannels. *Int. J. Comput. Fluid Dyn.* **2008**, *22*, 475–480. [CrossRef]

Disclaimer/Publisher's Note: The statements, opinions and data contained in all publications are solely those of the individual author(s) and contributor(s) and not of MDPI and/or the editor(s). MDPI and/or the editor(s) disclaim responsibility for any injury to people or property resulting from any ideas, methods, instructions or products referred to in the content.